Supporting Information

Chinese dumpling-like $NaTi_2(PO_4)_3$/MXene@Reduced Graphene for Capacitive deionization with High Capacity and Increased Cycling Stability

Xiaojie Shen[1, 2, 3, ‡], Yuecheng Xiong[4, 5, 6, ‡], Fei Yu[1*], Jie Ma[2,4*]

1 College of Marine Ecology and Environment, Shanghai Ocean University, Shanghai 201306, P.R. China, E-mail: fyu@vip.163.com

2 School of Civil Engineering, Kashi University, Kashi 844000, China

3 Marine Science and Technology College, Zhejiang Ocean University, Zhoushan 316004, P.R. China.

4 Research Center for Environmental Functional Materials, College of Environmental Science and Engineering, Tongji University, 1239 Siping Road, Shanghai 200092, P.R. China

5 Department of Chemistry, City University of Hong Kong, Kowloon, Hong Kong, China

6 Hong Kong Branch of National Precious Metals Material Engineering Research Center (NPMM), City University of Hong Kong, Kowloon, Hong Kong, China.

‡These authors contributed equally to this work.

Experimental methods

1 Preparation of 2D delaminated $Ti_3C_2T_x$ MXene

One gram of LiF (>98%) was dissolved in 20 mL of 9 M HCl. Then, 1 g of sieved Ti_3AlC_2 powders (400 mesh) was added. The mixture was kept at 40°C for 24 h under stirring with a magnetic stirrer. The resulting solid residue was washed several times with deionized water and centrifuged at a speed of 3500 rpm until the pH of the supernatant was approximately 6. The powder was mixed with deionized water and sonicated for 1 h under an ice-bath, through which Ar gas was bubbled. The resulting solution was centrifuged for 40 min at a speed of 4000 rpm. Finally, the 2D delaminated $Ti_3C_2T_x$ colloidal was obtained. To determine the volumetric density, a syringe was used to pull out 3 ml of the colloidal suspension to filter a film. The remaining suspension was stored in sealed bottles under Ar. After drying in air, it was weighed. For all the work conducted herein, the 2D delaminated $Ti_3C_2T_x$ MXene solution concentration was approximately 3 mg/mL.

2 Material characterization

Scanning electron microscopy (SEM, Hitachi 54800, Japan) and transmission electron microscopy (TEM, JEOL-2010F, Japan) were used to analyze the morphology and microstructure. The crystal structures were analyzed using X-ray diffraction (XRD, D8 Advance, Bruker, Germany) operated at 40 mA and 45 kV with Cu Kα radiation (λ=0.15418 nm, 5°/min, 3-65°). The Brunauer-Emmett-Teller (BET) isotherms and specific surface area (BET surface area) were obtained using a Belsorp Mini-Ⅱ instrument (Japan) at 77 K. The pore size distribution profile was analyzed using the Barrett-Joyner-Halenda (BJH) model. X-ray photoelectron spectroscopy (XPS Kratos Axis UltraDLD SHIMADZU, Japan) was performed using monochromated Al Ka X-rays at a base pressure of 1×10^{-9} Torr.

3 Electrochemical measurement

The AC EDL electrode consisted of 80% active material, 10% acetylene black and a 10% polyvinylidene difluoride (PVDF) binder in N-methyl-2-pyrrolidone (NMP) on a graphite sheet (mass ratio). Constant voltage (CV) and galvanostatic charging-discharging (GCD) tests were performed on a three-electrode electrochemical workstation (CHI660D, Chenhua Instruments Co., China), using Pt as the counter electrode, Ag/AgCl as the reference electrode, and 1 M NaCl as the electrolyte. The specific capacitance (C, F/g) can be obtained from the CV curves using the following equation:

$$C = \int idV/\Delta Vmv \qquad (1)$$

where i is the current (A), m is the mass of the active material (g), ΔV is the voltage window (V), and v is the scan rate (V/s).

Electrochemical impedance spectroscopy (EIS) was applied via a CHI660D instrument with a calomel reference electrode, and the data were obtained using a 5mV amplitude in the frequency range from 10^5 Hz to 0.1 Hz.

4 Desalination experiments

The electro-sorption experiments were conducted in a batch mode system with an HCDI unit cell, which included an activated carbon (AC) anode, an MXene cathode, an anion exchange membrane (AEM) and a cation exchange membrane (CEM). All the experiments were performed by applying a 30 mA/g electric current density with a flow rate of 50 ml/min, and the feed water was pumped through plastic tubes via a peristaltic pump. The conductivity of the solution was monitored by a conductivity meter (METTLER TOLEDO S230, Switzerland). The volume and temperature of the solution were maintained at 45 mL and 25°C, respectively. The relationship between the conductivity and the concentration was calibrated prior to the deionization experiments.

The desalination capacity (Γ), removal rates (v) and energy consumption (kWh/kg-NaCl) are defined as follows:

$$\Gamma = (C_0 - C_e) \times V/m_t \quad (2)$$

$$v = \frac{\Gamma}{t} \quad (3)$$

$$\text{Energy consumption} = \frac{i \times \int v\, dt}{3.6 \times (C_e - C_0) \times V} \quad (4)$$

where C_0 and C_e (mg/L) are the initial and final NaCl concentrations, respectively, m_t (g) is the mass of the MXene electrode, i is the current (A), and V (L) is the volume of the NaCl solution.

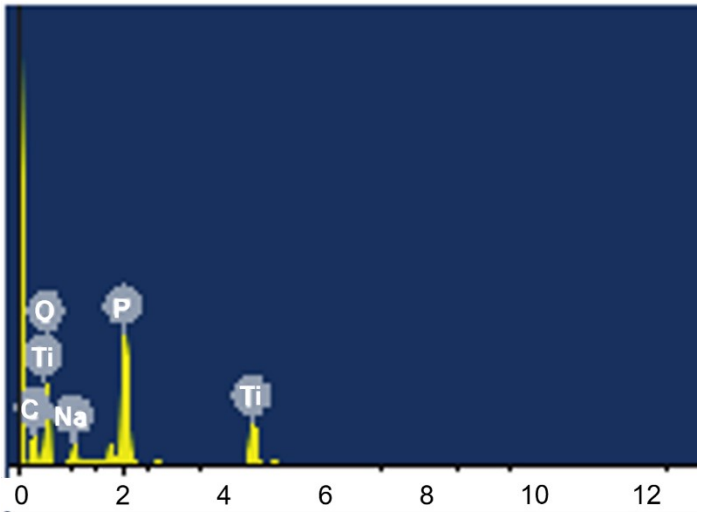

Figure S1. EDX spectra of M-NTP/rGO

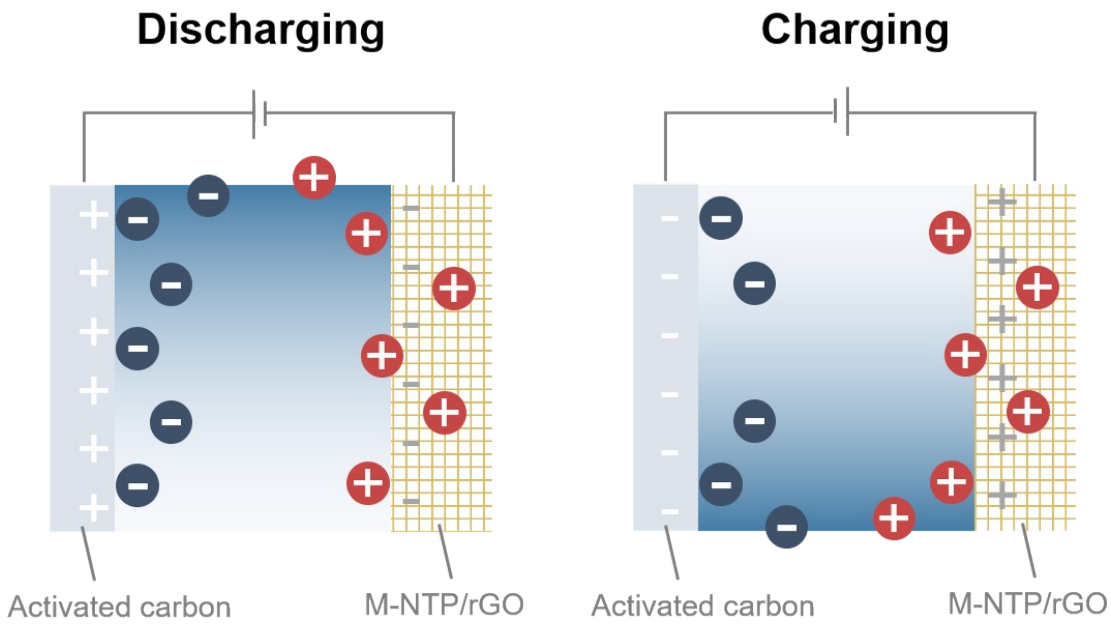

Figure S2. Demonstrative graph of discharging and charging process during repetitive capacitive deionization cycles.

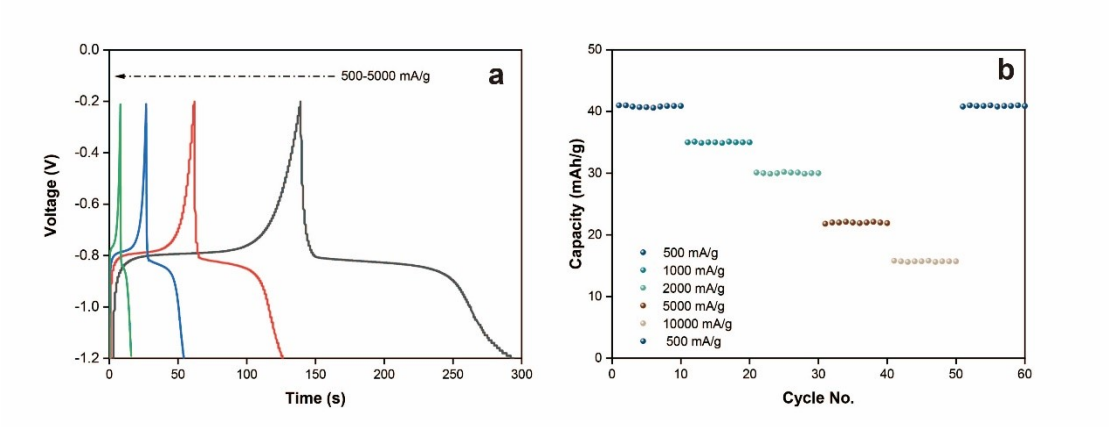

Figure S3. (a) Galvanostatic charging/discharging profiles of the M-NTP/rGO electrode at different specific currents. (b) Charging capacity of the M-NTP/rGO electrode at different specific currents.

Table S1 Comparison of desalination performance among advanced cathode materials in capacitive deionization.

Materials	**Applied voltage (V)**	**Initial NaCl concentration (ppm)**	**SAC ($mg_{NaCl}/g_{cathode}$)**	**SAR ($mg_{NaCl}/g_{cathode}$/min)**	**Operation cycles (with SAC retention rate if applicable)**	**Ref.**
M-NTP/rGO	**1.8, 50 mA g^{-1}**	**585**	**251.55**	**1.63**	**100 cycles (80%)**	**This work**
porous $Ti_3C_2T_x$	1.2	10,000	45	-	60 cycles (ca.93%)	[1]
L-S-$Ti_3C_2T_x$	1.6	292.5	72	1.66	50 cycles (90%)	[2]
$Ti_3C_2T_x$/NiHCF	1.4	500	85.1	15	50 cycles	[3]
$NaTi_2(PO_4)_3/Ti_3C_2T_x$	1.8	1000	128.6	29.6	20 cycles	[4]
Bi-ene NSs@MXene	1.2	1170	88.2	9	30 cycles	[5]
$Ti_3C_2T_x$-NTO/rGO	1.4	1000	57.6	1.14	100 cycles (87.3%)	[6]
PB/PANI	1.2	500	70	24	250 cycles	[7]
MoS_2/NOMC	1.6	250	28.82	0.48	10 cycles	[8]
$Ti_3C_2T_x$/mPDA	1.5	500	28.75	0.96	200 cycles	[9]
FeNiHCF@HGT	30 mA g^{-1}	1755	35	1.52	100 cycles (106.6%)	[10]
Antimonene	1.2	135	31.4	0.5	5 cycles	[11]
$TiO_2/Ti_3C_2T_x$	15 mA g^{-1}	500	75.62	1.3	60 cycles (94%)	[12]
Membrane-free capacitive deionization						
Hollow carbon@MnO_2	1.2	500	30.7	7.8	50 cycles (90.1%)	[13]
MnO_2//Ppy AC	1.4	850	34.15	18	50 cycles (80%)	[14]
AC//PTMA	1.2	250	13.9	5	20 cycles	[15]

Note: SAC, salt adsorption capacity; SAR, salt adsorption rate; PB, Prussian blue; PANI, polyaniline; NTO, sodium titanate; Bi-ene NSs, hierarchical bismuthene nanosheets; NOMC, nitrogen-doped highly ordered mesoporous carbon; mPDA, mesoporous polydopamine; HGT,

hollow graphite tube; Ppy AC, polypyrrole grafted activated carbon; PTMA, poly (2,2,6,6-tetramethylpiperidinyloxy methacrylate).

References

[1] Bao, W.; Tang, X.; Guo, X.; Choi, S.; Wang, C.; Gogotsi, Y.; Wang, G., Porous cryo-dried MXene for efficient capacitive deionization. *Joule* **2018,** *2*, (4), 778-787.

[2] Shen, X.; Xiong, Y.; Hai, R.; Yu, F.; Ma, J., All-MXene-Based Integrated Membrane Electrode Constructed using $Ti_3C_2T_x$ as an Intercalating Agent for High-Performance Desalination. *Environ. Sci. Technol.* **2020,** *54*, (7), 4554-4563.

[3] Wang, S.; Li, Z.; Wang, G.; Wang, Y.; Ling, Z.; Li, C., Freestanding Ti3C2T x MXene/Prussian Blue Analogues Films with Superior Ion Uptake for Efficient Capacitive Deionization by a Dual Pseudocapacitance Effect. *ACS Nano* **2021,** *16*, (1), 1239-1249.

[4] Chen, Z.; Xu, X.; Ding, Z.; Wang, K.; Sun, X.; Lu, T.; Konarova, M.; Eguchi, M.; Shapter, J. G.; Pan, L., Ti_3C_2 MXenes-derived $NaTi_2(PO_4)_3$/MXene nanohybrid for fast and efficient hybrid capacitive deionization performance. *Chem. Eng. J.* **2021,** *407*, 127148.

[5] Gong, S.; Liu, H.; Zhao, F.; Zhang, Y.; Xu, H.; Li, M.; Qi, J.; Wang, H.; Li, C.; Peng, W., Vertically aligned bismuthene nanosheets on MXene for high-performance capacitive deionization. *ACS Nano* **2023,** *17*, (5), 4843-4853.

[6] Shen, X.; Li, L.; Xiong, Y.; Yu, F.; Ma, J., Graphene-assisted Ti_3C_2 MXene-derived ultrathin sodium titanate for capacitive deionization with excellent rate performance and long cycling stability. *J. Mater. Chem. A* **2022,** *10*, (18), 10192-10200.

[7] Shi, W.; Liu, X.; Deng, T.; Huang, S.; Ding, M.; Miao, X.; Zhu, C.; Zhu, Y.; Liu, W.; Wu, F., Enabling superior sodium capture for efficient water desalination by a

tubular polyaniline decorated with Prussian blue nanocrystals. *Adv. Mater.* **2020,** *32*, (33), 1907404.

[8] Tian, S.; Zhang, X.; Zhang, Z., Novel MoS_2/NOMC electrodes with enhanced capacitive deionization performances. *Chem. Eng. J.* **2021,** *409*, 128200.

[9] Li, Q.; Xu, X.; Guo, J.; Hill, J. P.; Xu, H.; Xiang, L.; Li, C.; Yamauchi, Y.; Mai, Y., Two-dimensional MXene-polymer heterostructure with ordered in-plane mesochannels for high-performance capacitive deionization. *Angew. Chem. Int. Ed.* **2021,** *133*, (51), 26732-26738.

[10] Tang, Z.; Hu, B.; Nie, P.; Shang, X.; Yang, J.; Liu, J., Bimetallic Fe, Ni-PBA on hollow graphite tube for capacitive deionization with exceptional stability. *Chem. Eng. J.* **2023**, 143216.

[11] Gao, Y.; Lin, C.; Zhang, K.; Zhou, W.; Guo, S.; Liu, W.; Jiang, L.; Zhang, S.; Zeng, H., Pressurized alloying assisted synthesis of high quality antimonene for capacitive deionization. *Adv. Funct. Mater.* **2021,** *31*, (34), 2102766.

[12] Liu, N.; Yu, L.; Liu, B.; Yu, F.; Li, L.; Xiao, Y.; Yang, J.; Ma, J., Ti_3C_2-MXene Partially Derived Hierarchical 1D/2D TiO_2/Ti_3C_2 Heterostructure Electrode for High-Performance Capacitive Deionization. *Adv. Sci.* **2023,** *10*, (2), 2204041.

[13] Wang, S.; Wang, G.; Wu, T.; Li, C.; Wang, Y.; Pan, X.; Zhan, F.; Zhang, Y.; Wang, S.; Qiu, J., Membrane-Free Hybrid Capacitive Deionization System Based on Redox Reaction for High-Efficiency NaCl Removal. *Environ. Sci. Technol.* **2019,** *53*, (11), 6292-6301.

[14] Tan, G.; Lu, S.; Xu, N.; Gao, D.; Zhu, X., Pseudocapacitive Behaviors of

Polypyrrole Grafted Activated Carbon and MnO_2 Electrodes to Enable Fast and Efficient Membrane-Free Capacitive Deionization. *Environ. Sci. Technol.* **2020,** *54*, (9), 5843-5852.

[15] Li, Y.; Ding, Z.; Li, J.; Wang, K.; Lu, T.; Pan, L., Novel membrane-free hybrid capacitive deionization with a radical polymer anode for stable desalination. *Desalination* **2020,** *481*, 114379.